# Exploring Inhomogeneous Kibble-Zurek Mechanism in a Spin-Orbit Coupled Bose-Einstein Condensate

Chang-Rui Yi,[1,2,3,*] Sheng Liu,[2,4,*] Rui-Heng Jiao,[1,2,3] Jin-Yi Zhang,[1,2,3,†] Yong-Sheng Zhang,[2,4,‡] and Shuai Chen[1,2,3,§]

[1]*Hefei National Laboratory for Physical Sciences at the Microscale and Department of Modern Physics, University of Science and Technology of China, Hefei, Anhui 230026, China*

[2]*CAS Center for Excellence in Quantum Information and Quantum Physics, University of Science and Technology of China, Anhui 230026, China*

[3]*Shanghai Research Center for Quantum Science, Shanghai 201315, China*

[4]*CAS Key Laboratory of Quantum Information, University of Science and Technology of China, Hefei 230026, China*

(Received 3 September 2020; revised 10 November 2020; accepted 9 December 2020; published 28 December 2020)

The famous Kibble-Zurek mechanism offers us a significant clue to study quantum phase transitions out of equilibrium. Here, we investigate an intriguing phenomenon of a spin-orbit coupled Bose-Einstein condensate by quenching the Raman coupling strength from a high-symmetry phase (nonmagnetic phase) to a low-symmetry phase (magnetic phase). When crossing the critical point, the fluctuation of momentum distribution leads to delayed bifurcation structures. Simultaneously, the domain information emerges in momentum space. Moreover, the universal scalings of spatiotemporal dynamics are extracted from the fluctuations and domains, which manifests homogeneous and inhomogeneous Kibble-Zurek power laws at different timescales. Our work demonstrates a paradigmatic study on the inhomogeneous Kibble-Zurek mechanism.

DOI: 10.1103/PhysRevLett.125.260603

*Introduction.*—The nonequilibrium phase transition is an intriguing and ubiquitous phenomenon in nature, ranging from cosmology and condensed matter to ultracold atom systems. Understanding such a phenomenon is one of the most challenging problems in modern physics. Only a few tools have emerged for elaborating a nonequilibrium critical phenomenon. The remarkable Kibble-Zurek mechanism (KZM) [1,2] is one paradigm of the tools to depict a dynamic phase transition, modeling the critical slowing-down phenomenon [3,4] and the formation of topological defects in spontaneous continuous symmetry-breaking phase transitions by universal power-law scalings.

The KZM was originally introduced in the evolution of the early Universe [1]. It has been experimentally investigated for both classical and quantum phase transitions in a wide variety of systems, such as cosmic microwave background [5], liquid helium [6,7], superconductor [8,9], liquid crystals [10], and colloidal monolayers [11]. Recently, the KZM has also been extended to ultracold atoms [12–22]. Until now, most experiments are mainly demonstrated on a homogeneous phase transition, while inhomogeneity of the system is omnipresent; thus, the inhomogeneous phase transition is a generic problem. Theoretical works unravel that inhomogeneity can induce the suppression effect of topological defects across a phase transition [23–35], beneficial to exploring the adiabatic preparation of a qubit and realizing feasible protocols for adiabatic quantum computation [36]. Currently, such an inhomogeneous mechanism has been far less investigated in experiments (see ion trap systems in Refs. [37,38] and cold atom systems in Refs. [16,20,24]). Here, the main difficulty in testing the inhomogeneous KZM is that extracting the power-law exponents requires tuning the quench rate over orders of magnitude to obtain an adequate signal. The advent of the Raman-induced spin-orbit (SO) coupled Bose-Einstein condensate (BEC) [39–42] renders a new test bed with a well-controlled feature for exploring dynamic quantum phase transitions in ultracold atom systems.

In this Letter, we study the inhomogeneous KZM with a Raman-induced one-dimensional (1D) SO coupled BEC. This system possesses three phases: the stripe phase, magnetized phase (MP), and nonmagnetized phase (NMP) [42–44]. Crossing from the NMP to the MP is a second-order quantum phase transition [43,45]. This transition occurs when the Raman coupling strength goes down across a critical value, which gives rise to the system entering the magnetic order phase, and breaks a $Z_2$ symmetry. In the experiment, we carry out quench dynamics via tuning Raman coupling strength from the NMP to the MP. The fluctuation of momentum distribution and the correlation length are measured, whereby quench rates are varied by 3 orders of magnitude. Across the critical point, delayed bifurcation structure of momentum distribution is observed. The fluctuation of

 © 2020 American Physical Society

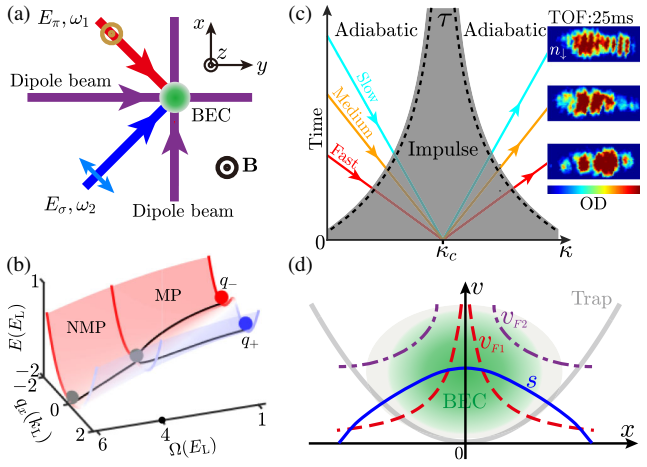


FIG. 1. KZM with a Raman-induced 1D SO coupled BEC. (a) Setup for a 1D SO coupled BEC. The orthogonal red ($E_\pi$) and blue ($E_\sigma$) beams construct Raman coupling. (b) Second-order quantum phase transition occurs from the nonmagnetized phase, through the critical point $\Omega_c = 4E_L$, to the magnetized phase with two minima at $q_x = q_\pm$. (c) The sketch of the KZM, displaying three stages: two adiabatic stages and an impulse stage. Domain structures are shown for three different quench rates in momentum space. (d) The sketch of the inhomogeneous KZM. The BEC stays in a trap (gray). The blue solid, red dashed, and purple dashed curves denote velocity of sound $s$ and the velocity of the propagation front of the phase transition $v_{F1}$ with large $\tau_q$ and $v_{F2}$ with small $\tau_q$, respectively.

momentum distribution collapses into a single curve via rescaling the time, satisfying the universality hypothesis [4]. We acquire the correlation length from the momentum distribution as well, indicating the emergence of domain structures. Furthermore, the power-law scalings of characteristic time and length are extracted, manifesting the inhomogeneous Kibble-Zurek mechanism.

*The system and KZM.*—Our experiments are based on a Raman-induced 1D SO coupled BEC of $^{87}$Rb, produced in the crossed dipole trap, as sketched in Fig. 1(a). A bias magnetic field $\mathbf{B} \approx 14.5$ G is applied in t he $\hat{z}$ direction, giving the quantization axis and Zeeman splitting of 10.2 MHz. Two Raman beams with wavelength $\lambda = 787$ nm shine on the BEC and couple magnetic sublevels $|1,-1\rangle$ (spin up $|\uparrow\rangle$) and $|1,0\rangle$ (spin down $|\downarrow\rangle$) in $F = 1$ manifolds to form spin-momentum locking along the $\hat{x}$ direction. The Hamiltonian reads ($\hbar = 1$)

$$H = \frac{(q_x - k_L\sigma_z)^2}{2m} + \frac{\Omega}{2}\sigma_x + \frac{\delta}{2}\sigma_z + H_I, \qquad (1)$$

where $m$, $\sigma_{x,z}$, $\Omega$, $\delta$, $k_L$, and $H_I$ are the atomic mass, Pauli matrices, Raman coupling strength, two-photon Raman detuning, recoil momentum, and interaction, respectively. Here, we focus on the case $\delta = 0$. The single-particle dispersion $E(q_x)$ for different strengths $\Omega$ is shown in Fig. 1(b). For $\Omega < 4E_L$ ($E_L = k_L^2/2m$, $k_L = \sqrt{2}\pi/\lambda$), $E(q_x)$ has two local minima, and bosons condense in one of the minima, i.e., the MP, which spontaneously breaks a $Z_2$ symmetry and has nonzero magnetization. Whereas for $\Omega > 4E_L$, $E(q_x)$ has only one minimum, i.e., the NMP [42–44]. The interaction $H_I$ of the two-component condensate includes spin-independent interaction $c_0 = g_{\uparrow\uparrow}$ and spin-dependent interaction $c_2 = g_{\uparrow\downarrow} - g_{\uparrow\uparrow}$, where $g_{ij} = 4\pi N a_{ij}/m$ is the interaction strength with $a_{ij}$ ($i, j = \uparrow, \downarrow$) being the scattering length and $N$ being the atom number [46]. After minimizing the total energy, one obtains the phase diagram. Thus, the system undergoes a continuous quantum phase transition from the NMP to the MP. The transition point is modified by $c_2$. In our case, the shifted value is negligible due to small $|c_2|$ and low density of the condensate; see [43,47] for details.

In Fig. 1(c), the general KZM is delineated. Here, the dynamics of spontaneous symmetry breaking induced by a control parameter $\kappa$ is considered. From the critical phenomena, a second-order phase transition is characterized by the divergence of both equilibrium correlation length $\xi \sim |\varepsilon|^{-\nu}$ and equilibrium relaxation time $\tau \sim |\varepsilon|^{-z\nu}$, where the critical exponent $\nu$ and dynamic critical exponent $z$ are determined by the universality class of the phase transition [4]. $\varepsilon = (\kappa_c - \kappa)/\kappa_c$ is the reduced distance to critical point $\kappa_c$.

The KZM describes the critical dynamics by three stages: an adiabatic stage far away from critical point; a frozen stage (impulse stage) in the vicinity of the critical point, where the system is effectively frozen due to the divergence of relaxation time (critical slowing-down phenomenon); and another adiabatic stage with a broken symmetry phase [see Fig. 1(c)]. Within the frozen stage, the system hardly follows the ground state of its instantaneous Hamiltonian. It unfreezes only at a delayed time after passing the critical point. For a finite linear quench $\varepsilon(t) = t/\tau_q$ (quench time $\tau_q$), freeze-out occurs when $\tau$ is comparable to the timescale of the quench, i.e., $\tau \sim \varepsilon(t)/\dot{\varepsilon}(t)$. Thus, frozen time (delay time) $t_d \sim \tau_q^{\nu z/(1+z\nu)}$. Meanwhile, when it unfreezes, topological defects form, and the average size of topological defects is determined by $\xi \sim \tau_q^{\nu/(1+z\nu)}$.

But the inhomogeneity in a system leads to a spatial dependence of the critical point $\kappa_c(x)$ and the local quench time $\tau_q(x)$. As a result, the phase transition does not occur simultaneously in the whole system, and the homogeneous KZM described above breaks down, giving rise to different scaling laws for the number of defects as a function of the quench time.

When the critical point is locally reached, there exists a causal horizon related to the velocity of sound $s$ and the propagation front of the phase transition $v_F$ [23,25–35]. And $s$ at frozen time and $v_F$ are estimated as

$$s = \frac{\xi}{\tau} \sim [\tau_q(x)]^{-[\nu(z-1)]/(1+\nu z)},$$
$$v_F = \left|\frac{dx_F}{dt_F}\right| = \left|\frac{d\tau_q(x)}{dx_F}\right|^{-1}, \quad (2)$$

respectively, where $x_F$ and $t_F$ represent the location and time of finding the front, respectively. For a homogeneous system, $v_F$ diverges. To form defects, $s < v_F$ is required. Therefore, in a homogeneous system, defects always emerge. Nevertheless, in an inhomogeneous system, the phase transition does not occur simultaneously in the whole system, when $s > v_F$ information can propagate from a low-symmetry to a high-symmetry phase. This exchange of information affects the choice of the high-symmetry phase, suppressing the formation of defects. Specifically, regarding fast quenches, the number of defects is well predicted by a power-law scaling in agreement with the homogeneous KZM due to $v_{F2} > s$ everywhere [Fig. 1(d)]. Regarding slow quenches, there exists novel power-law scaling behavior of the number of defects, characterized by a larger exponent due to $v_{F1} < s$ in certain locations [Fig. 1(d)]. Alternatively, local drive gives rise to a more noticeable suppression of defect formation. Hence, for a wide range of quench rate, turning behavior of exponents is exhibited.

*Quenches and bifurcated structures of the momentum distribution.*—In the experiment, we vary Raman coupling to explore the dynamical quantum phase transition. First, the BEC of about $2 \times 10^5$ atoms is produced in $|\uparrow\rangle$. Then we adiabatically increase the strength $\Omega$ to the initial Raman coupling $\Omega_i = 5.0E_L$; thus, the BEC is prepared in the ground state of NMP, i.e., $1/\sqrt{2}(|\uparrow, q_x = 0\rangle + |\downarrow, q_x = 0\rangle)$. Finally, Raman coupling is linearly quenched from $\Omega_i = 5.0E_L$ to the final Raman coupling strength $\Omega_f = 2.0E_L$ with different quench times $\tau_q$ to carry out the measurements. Meanwhile, detuning $\delta$ keeps to 0, guaranteed by a stable magnetic field [48]. For detection, we apply the spin-resolved time of flight (TOF) of 25 ms and image along the $\hat{z}$ direction to record the momentum distribution of atom clouds in spin up $n_\uparrow(\boldsymbol{q})$ and spin down $n_\downarrow(\boldsymbol{q})$.

Momentum distributions of the atoms $n(\boldsymbol{q}, t) = n_\uparrow(\boldsymbol{q}, t) + n_\downarrow(\boldsymbol{q}, t)$ with different $\tau_q$ are shown in Fig. 2. For $\Omega > \Omega_c$, the atoms are at quasimomentum $\boldsymbol{q} = 0$. For $\Omega < \Omega_c$, the atoms form a delayed bifurcated structure as $\Omega$ ramps down. Meanwhile, the domain structures are also observed, whereafter the atoms are again distributed adiabatically at $\Omega = 2E_L$ if $\tau_q$ is large enough. As $\tau_q$ is gradually increased, the bifurcation point is approaching the equilibrium value. The bifurcation structure of the quasiadiabatic state is also plotted as a benchmark, reflecting the bifurcation point exactly as the critical point at $\Omega_c = 4E_L$.

*Temporal scaling.*—To quantitatively investigate the temporal scaling of the delayed bifurcation structures, we describe the fluctuation of momentum distribution by its standard deviation

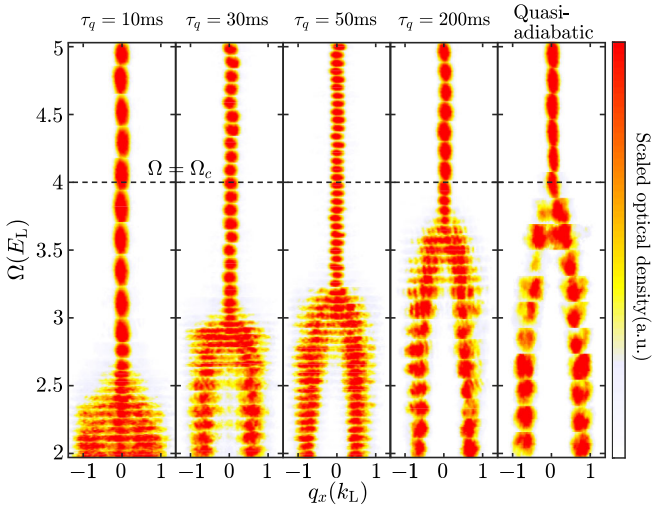


FIG. 2. Delayed bifurcation structures of momentum distribution as a function of the strength $\Omega$ in the dynamic quantum phase transition. The photos of momentum distribution with different $\Omega$ are arranged together for a fixed $\tau_q$. From left to right, bifurcation structures for quench time $\tau_q = 10$, 30, 50, and 200 ms equilibrium state, respectively.

$$\zeta(t) = \sqrt{\frac{\int q_x^2 n(q_x, t) dq_x}{\int n(q_x, t) dq_x} - \frac{[\int q_x n(q_x, t) dq_x]^2}{[\int n(q_x, t) dq_x]^2}}, \quad (3)$$

where $n(q_x, t) = \sum_{q_y} [n_\uparrow(\boldsymbol{q}, t) + n_\downarrow(\boldsymbol{q}, t)]$. For comparison, among different $\tau_q$, $\zeta(t)$ is normalized as $Z(t) = [\zeta(t) - \zeta_{\min}]/(\zeta_{\max} - \zeta_{\min})$, where $\zeta_{\max}$ ($\zeta_{\min}$) is the maximum (minimum) of $\zeta(t)$.

In Fig. 3(a), $Z(t)$ is plotted as a function of time $t$ with different $\tau_q$. As can be seen, the dynamics of $Z(t)$ can be depicted in three stages over a wide range of $\tau_q$. First, below the critical point $\Omega_c$, $Z(t)$ does not grow. Second, just after passing $\Omega_c$, the system is dominated by a critical slowing-down phenomenon, and $Z(t)$ remains low. The system enters the impulse stage. Finally, $Z(t)$ increases and saturates, since the system unfreezes. The rapid growth of $Z(t)$ signifies the emergence of domains in our system. The saturation of $Z(t)$ implies the system evolves adiabatically again.

According to the growth behavior of $Z(t)$, an empirical sigmoid function is applied to fit the data [47]. When the system unfreezes, to characterize the delay time $t_d$, we set $Z(t_d) = 0.5$ based on the fitting function of $Z(t)$ [see Fig. 3(a), black dashed line parallelling the horizontal axis]; thus, $t_d$ is figured out for different $\tau_q$. In Fig. 3(b), we plot $t_d$ as a function of $\tau_q$ in log-log scale. It is obvious to see that there are two power-law scalings, and the turning range is around 20–50 ms. A linear fit in the log-log scale gives the exponent of $\alpha_1 = 0.55(2)$ and $\alpha_2 = 0.97(3)$, respectively. We complement these measurements with numerical simulations based on a truncated Wigner method with the Gross-Pitaveskii equation (GPE) (see [47,49] for details),

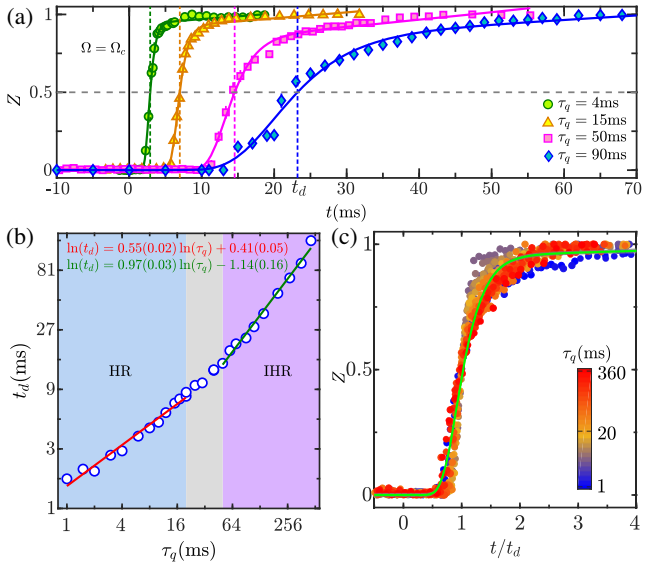


FIG. 3. Standard deviation of momentum distribution in the dynamic quantum phase transition. (a) Standard deviation of momentum distribution $Z$ as a function of time $t$ for different quench times $\tau_q$. The solid curves are based on the sigmoid function. (b) The dependence of $t_d$ (circles) on the quench time $\tau_q$ is well fit by power laws (solid curves) with two different scaling exponents: $\alpha_1 = 0.55(2)$ in the homogeneous region (HR, light cyan) and $\alpha_2 = 0.97(3)$ in the inhomogeneous region (IHR, purple). (c) Standard deviation for 24 quench times from $\tau_q =$ 1 ms to $\tau_q = 360$ ms collapse into a single curve when time is scaled by $t_d$. The solid curve shows the best fit based on the sigmoid fitting function.

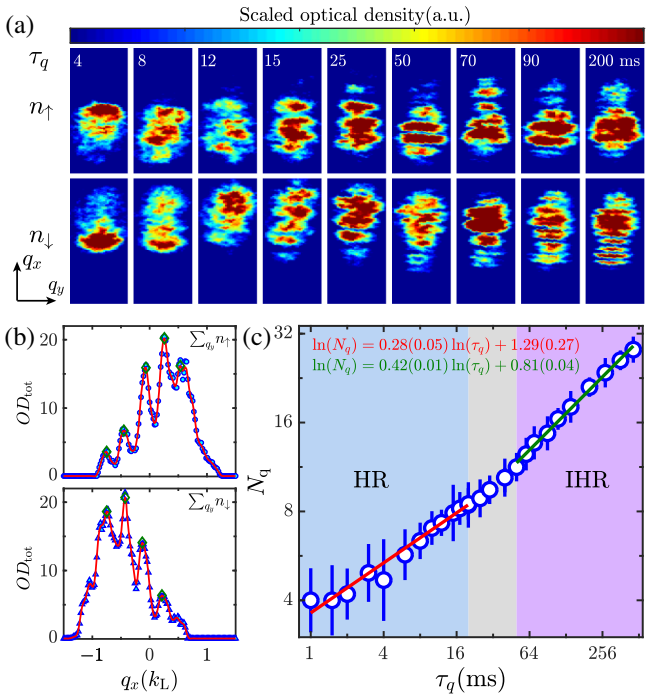


FIG. 4. Spatial correlations in the dynamic quantum phase transition. (a) Domain structure of spin-up (top row) and spin-down (lower row) images near the time $t = 1.1t_d$ at different quench times $\tau_q$. (b) Column-integrated momentum distribution of $n_\uparrow$ and $n_\downarrow$ for quench time $\tau_q = 25$ ms. $OD_{\rm tot}$ is the sum of optical density along the $q_y$ direction. The circles (triangles) denote experimental data of $n_\uparrow$ ($n_\downarrow$). The red solid curves are based on numerical smoothing. Each green diamond is a peak, i.e., a domain. (c) Domain numbers in momentum space $N_q$ (circles) as a function of $\tau_q$ in log-log scale. $N_q$ is the sum of domain numbers in $n_\uparrow$ and $n_\downarrow$. The two solid lines are linear fitting lines, giving spatial scaling exponents $\beta_1 = 0.28(5)$ in the HR (cyan) and $\beta_2 = 0.42(1)$ in the IHR (purple).

giving $\alpha_1 = 0.50(2)$ and $\alpha_2 = 1.02(3)$, respectively, in good agreement with the experimental data. After rescaling time $t$ by $t/t_d$, all the $Z(t)$ curves approximately collapse into a single curve, shown in Fig. 3(c), satisfying the universality hypothesis [4]. The exponent $\alpha_1 = 0.55(2)$ basically satisfies the homogeneous KZM, since the mean field theory gives $\nu = 1/2$, $z = 2$, and, thus, $\alpha_1 = \nu z/(1 + z\nu) = 1/2$.

In Fig. 3(c), the system demonstrates the inhomogeneous KZM with a larger exponent $\alpha_2 = 0.97(3)$. Here, the harmonic trap plays a primary reason for providing inhomogeneity, while spin-dependent interaction $c_2$ is responsible for the simultaneous observation of homogeneous and inhomogeneous KZ phenomena. Specifically, the harmonic trap gives the spatial-dependent density, together with Raman coupling, which leads to the local critical point and local speed of sound. The speed of sound is estimated as $s \sim \sqrt{G_1(x)/m^*}$, where $G_1(x)$ denotes the interaction strength and $m^*$ is the effective mass modulated by spin-orbit coupling [50]. Meanwhile, the local critical point implies a local speed of front $v_F \sim (\Omega_i - \Omega_f)R_x^2/(|c_2|\tau_q x)$, where $\Omega_i$ ($\Omega_f$) is Raman coupling in the NMP (MP) and $R_x$ is the Thomas-Fermi radius along the $\hat{x}$ direction. In our system, $c_2 = -3.61 \times 10^{-14}$ Hz cm$^3$, and the peak density of condensate is around $10^{13}$/ cm$^3$; along with Raman coupling, those ingredients render $s > v_F$ when $\tau_q$ exceeds 20–50 ms (see [47] for details). Thus, according to the inhomogeneous KZM, the system enters the inhomogeneous region, and a larger exponent is observed.

*Spatial scaling.*—For the spatial scaling, we investigate the domain information in momentum space by adopting the same experimental protocol as temporal scaling. To characterize the domain information, it is appropriate to define a correlation function $G(\mathbf{s})$ with correlation length $\xi$ as the width of $G(\mathbf{s})$. Furthermore, one can obtain that $G(\mathbf{s})$ is the Fourier transform of the momentum distribution $P(\mathbf{p})$ with $\xi \sim \hbar/\Delta p$ ($\Delta p$ is momentum dispersion) [47,51]. Hence, in the experiment, it is convenient to perform spin-resolved TOF to extract $\xi$.

In Fig. 4(a), typical domain structures in momentum space are shown with different quench times $\tau_q$. Domain numbers of momentum space $N_q$ clearly depend on $\tau_q$. Qualitatively, for fast quench (for instance, $\tau_q = 4$ ms), the

size of domains is relatively large, and, thus, $N_q$ is little. For slower quench, the size of domains decreases with $\tau_q$, signifying more domain appearing in momentum space. In Fig. 4(b), we plot column-integrated momentum distribution of spin up and down for $\tau_q = 25$ ms to quantify the domains. A multiple-peak structure in momentum space is exhibited, reflecting the interplay of different defects in real space after the TOF. We define the number of peaks as domain numbers in momentum space $N_q$ and the width of single peak $\overline{\Delta p}$ as the average size of the domain. After the TOF, one has $\overline{\Delta p} \sim \hbar t_{\mathrm{TOF}}/m\xi$ [52], and the total width of the momentum distribution is $\hbar/L$, where $t_{\mathrm{TOF}} = 25$ ms and $L$ is the total sample width in real space. Thus, one obtains $N_q \propto \xi$ (see [47] for details).

$N_q$ as a function of $\tau_q$ are plotted in Fig. 4(c). A linear fit in the log-log scale gives the exponent of $\beta_1 = 0.28(5)$, basically satisfying the mean field theory $\beta_1 = 1/4$ for the homogeneous KZM, and $\beta_2 = 0.42(1)$, corresponding to the inhomogeneous KZM. Meanwhile, the fit indicates that the turning range is also around 20–50 ms, matching the position we obtained in temporal scaling. The exponents numerically extracted by GPE give $\beta_1 = 0.30(7)$ and $\beta_2 = 0.45(4)$; for details, see [47].

*Conclusion.*—In conclusion, we uncover a dynamics of quantum phase transition in a SO coupled BEC. Quenching through the critical point from the NMP to the MP displays the delayed bifurcation structures of momentum distribution. Moreover, spin domain information is also extracted from momentum distribution. The measured spatiotemporal scalings possess turning behavior, and the exponents are in agreement with the predictions of the homogeneous and inhomogeneous KZM with different quench times. For our spin-1/2 system, by applying adiabatic quenches with the inhomogeneous KZM, qubit states might be prepared and provide a fundamental idea for adiabatic quantum computation [36,53]. Besides, our work also paves the way to study spin domain coarsening dynamics (phase ordering kinetics) [54,55] in a SO coupled BEC, and coarsening dynamics with such a quantum system can serve as a fertile ground to study far-from-equilibrium physics.

We thank Xiang-Can Cheng for comments on the manuscript. This work was supported by the National Key R&D Program of China (No. 2016YFA0301601, No. 2016YFA0301300, and No. 2016YFA0501700); the National Natural Science Foundation of China (No. 11604321, No. 11674306, and No. 61590932); Anhui Initiative in Quantum Information Technologies (AHY120000); Shanghai Municipal Science and Technology Major Project (Grant No. 2019SHZDZX01); and the Strategic Priority Research Program of Chinese Academy of Science (Grant No. XDB28000000).

*These authors contributed equally to this work.
†jinyizhang1@gmail.com
‡yshzhang@ustc.edu.cn
§shuai@ustc.edu.cn

[1] T. W. B. Kibble, J. Phys. A **9**, 1387 (1976).
[2] W. H. Zurek, Nature (London) **317**, 505 (1985).
[3] L. P. Kadanoff, W. Götze, D. Hamblen, R. Hecht, E. A. S. Lewis, V. V. Palciauskas, M. Rayl, J. Swift, D. Aspnes, and J. Kane, Rev. Mod. Phys. **39**, 395 (1967).
[4] P. C. Hohenberg and B. I. Halperin, Rev. Mod. Phys. **49**, 435 (1977).
[5] N. Bevis, M. Hindmarsh, M. Kunz, and J. Urrestilla, Phys. Rev. Lett. **100**, 021301 (2008).
[6] C. Bäuerle, Y. M. Bunkov, S. N. Fisher, H. Godfrin, and G. R. Pickett, Nature (London) **382**, 332 (1996).
[7] V. M. H. Ruutu, V. B. Eltsov, A. J. Gill, T. W. B. Kibble, M. Krusius, Y. G. Makhlin, B. Plaçais, G. E. Volovik, and W. Xu, Nature (London) **382**, 334 (1996).
[8] R. Carmi, E. Polturak, and G. Koren, Phys. Rev. Lett. **84**, 4966 (2000).
[9] R. Monaco, J. Mygind, and R. J. Rivers, Phys. Rev. Lett. **89**, 080603 (2002).
[10] I. Chuang, R. Durrer, N. Turok, and B. Yurke, Science **251**, 1336 (1991).
[11] S. Deutschländer, P. Dillmann, G. Maret, and P. Keim, Proc. Natl. Acad. Sci. U.S.A. **112**, 6925 (2015).
[12] L. E. Sadler, J. M. Higbie, S. R. Leslie, M. Vengalattore, and D. M. Stamper-Kurn, Nature (London) **443**, 312 (2006).
[13] T. Donner, S. Ritter, T. Bourdel, A. Ottl, M. Kohl, and T. Esslinger, Science **315**, 1556 (2007).
[14] C. N. Weiler, T. W. Neely, D. R. Scherer, A. S. Bradley, M. J. Davis, and B. P. Anderson, Nature (London) **455**, 948 (2008).
[15] D. Chen, M. White, C. Borries, and B. DeMarco, Phys. Rev. Lett. **106**, 235304 (2011).
[16] G. Lamporesi, S. Donadello, S. Serafini, F. Dalfovo, and G. Ferrari, Nat. Phys. **9**, 656 (2013).
[17] E. Nicklas, M. Karl, M. Höfer, A. Johnson, W. Muessel, H. Strobel, J. Tomkovič, T. Gasenzer, and M. K. Oberthaler, Phys. Rev. Lett. **115**, 245301 (2015).
[18] N. Navon, A. L. Gaunt, R. P. Smith, and Z. Hadzibabic, Science **347**, 167 (2015).
[19] L. W. Clark, L. Feng, and C. Chin, Science **354**, 606 (2016).
[20] B. Ko, J. W. Park, and Y. Shin, Nat. Phys. **15**, 1227 (2019).
[21] X.-P. Liu, X.-C. Yao, Y. Deng, X.-Q. Wang, Y.-X. Wang, X.-P. Li, Y.-A. Chen, and J.-W. Pan, arXiv:1902.07558.
[22] A. Keesling, A. Omran, H. Levine, H. Bernien, H. Pichler, S. Choi, R. Samajdar, S. Schwartz, P. Silvi, S. Sachdev, P. Zoller, M. Endres, M. Greiner, V. Vuletić, and M. D. Lukin, Nature (London) **568**, 207 (2019).
[23] J. Gauntlett, *Symmetry and Fundamental Physics: Tom Kibble at 80* (World Scientific, Singapore, 2014).
[24] H. Saito, Y. Kawaguchi, and M. Ueda, J. Phys. Condens. Matter **25**, 404212 (2013).
[25] T. W. Kibble and G. E. Volovik, JETP Lett. **65**, 102 (1997).
[26] J. Dziarmaga, P. Laguna, and W. H. Zurek, Phys. Rev. Lett. **82**, 4749 (1999).
[27] J. Dziarmaga and M. M. Rams, New J. Phys. **12**, 055007 (2010).
[28] J. Sabbatini, W. H. Zurek, and M. J. Davis, New J. Phys. **14**, 095030 (2012).

[29] A. del Campo, T. W. B. Kibble, and W. H. Zurek, J. Phys. Condens. Matter **25**, 404210 (2013).
[30] W. H. Zurek, Phys. Rev. Lett. **102**, 105702 (2009).
[31] A. del Campo, A. Retzker, and M. B. Plenio, New J. Phys. **13**, 083022 (2011).
[32] J. Sabbatini, W. H. Zurek, and M. J. Davis, Phys. Rev. Lett. **107**, 230402 (2011).
[33] F. J. Gómez-Ruiz and A. del Campo, Phys. Rev. Lett. **122**, 080604 (2019).
[34] D. Sadhukhan, A. Sinha, A. Francuz, J. Stefaniak, M. M. Rams, J. Dziarmaga, and W. H. Zurek, Phys. Rev. B **101**, 144429 (2020).
[35] S. Liu and Y. Zhang, Phys. Rev. A **99**, 053609 (2019).
[36] T. Albash and D. A. Lidar, Rev. Mod. Phys. **90**, 015002 (2018).
[37] S. Ulm, J. Roßnagel, G. Jacob, C. Degünther, S. T. Dawkins, U. G. Poschinger, R. Nigmatullin, A. Retzker, M. B. Plenio, F. Schmidt-Kaler, and K. Singer, Nat. Commun. **4**, 2290 (2013).
[38] K. Pyka, J. Keller, H. L. Partner, R. Nigmatullin, T. Burgermeister, D. M. Meier, K. Kuhlmann, A. Retzker, M. B. Plenio, W. H. Zurek, A. del Campo, and T. E. Mehlstäubler, Nat. Commun. **4**, 2291 (2013).
[39] Y.-J. Lin, K. Jiménez-García, and I. B. Spielman, Nature (London) **471**, 83 (2011).
[40] P. Wang, Z.-Q. Yu, Z. Fu, J. Miao, L. Huang, S. Chai, H. Zhai, and J. Zhang, Phys. Rev. Lett. **109**, 095301 (2012).
[41] L. W. Cheuk, A. T. Sommer, Z. Hadzibabic, T. Yefsah, W. S. Bakr, and M. W. Zwierlein, Phys. Rev. Lett. **109**, 095302 (2012).
[42] J.-Y. Zhang, S.-C. Ji, Z. Chen, L. Zhang, Z.-D. Du, B. Yan, G.-S. Pan, B. Zhao, Y.-J. Deng, H. Zhai, S. Chen, and J.-W. Pan, Phys. Rev. Lett. **109**, 115301 (2012).
[43] Y. Li, L. P. Pitaevskii, and S. Stringari, Phys. Rev. Lett. **108**, 225301 (2012).
[44] S.-C. Ji, J.-Y. Zhang, L. Zhang, Z.-D. Du, W. Zheng, Y.-J. Deng, H. Zhai, S. Chen, and J.-W. Pan, Nat. Phys. **10**, 314 (2014).
[45] C. Hamner, C. Qu, Y. Zhang, J. Chang, M. Gong, C. Zhang, and P. Engels, Nat. Commun. **5**, 4023 (2014).
[46] T.-L. Ho, Phys. Rev. Lett. **81**, 742 (1998).
[47] See Supplemental Material at http://link.aps.org/supplemental/10.1103/PhysRevLett.125.260603 for more details of the experimental protocol, the data analyzing and the numerical simulation.
[48] X.-T. Xu, Z.-Y. Wang, R.-H. Jiao, C.-R. Yi, W. Sun, and S. Chen, Rev. Sci. Instrum. **90**, 054708 (2019).
[49] L. A. Williamson and P. B. Blakie, Phys. Rev. A **94**, 023608 (2016).
[50] G. I. Martone, Y. Li, L. P. Pitaevskii, and S. Stringari, Phys. Rev. A **86**, 063621 (2012).
[51] C. Cohen-Tannoudji *et al.*, *Advances in Atomic Physics: an Overview* (World Scientific, Singapore, 2011), Chap. 17.
[52] L. Pitaevski and S. Stringari, *Bose-Einstein Condensation and Superfluidity* (Oxford University Press, Oxford, 2016).
[53] T. M. Hoang, H. M. Bharath, M. J. Boguslawski, M. Anquez, B. A. Robbins, and M. S. Chapman, Proc. Natl. Acad. Sci. U.S.A. **113**, 9475 (2016).
[54] A. Bray, Adv. Phys. **43**, 357 (1994).
[55] J. Hofmann, S. S. Natu, and S. Das Sarma, Phys. Rev. Lett. **113**, 095702 (2014).